Biosensors and Bioelectronics 144 (2019) 111694

Contents lists available at ScienceDirect

Biosensors and Bioelectronics

journal homepage: www.elsevier.com/locate/bios

Sensitive electrochemical detection of amyloid beta peptide in human serum using an interdigitated chain-shaped electrode

Hien T. Ngoc Le[a], Jinsoo Park[b], Somasekhar R. Chinnadayyala[a], Sungbo Cho[a,b,*]

[a] Department of Electronic Engineering, Gachon University, Seongnam-si, Gyeonggi-do, 13120, South Korea
[b] Department of Health Sciences and Technology, GAIHST, Gachon University, Incheon, 21999, Republic of Korea

ARTICLE INFO

Keywords:
Interdigitated chain-shaped electrode
Amyloid-β 1–42 peptide
anti-aβ antibody
Self-assembled monolayer
Electrochemical biosensor
Electrochemical impedance spectroscopy

ABSTRACT

In this study, we developed a small size, low cost, highly sensitive electrochemical biosensor with a low limit of detection by immobilizing specific anti-amyloid-β (aβ) antibody onto a self-assembled monolayer functionalized interdigitated chain-shaped electrode (anti-aβ/EDC–NHS/SAM/ICE). The anti-aβ/EDC–NHS/SAM/ICE specifically detects aβ 1–42 peptide (a peptide 1–42 amino acids long), which is one of main biomarkers of Alzheimer's disease in human serum (HS). Electrochemical impedance spectroscopy (EIS) was used to characterize the impedance change of the anti-aβ/EDC–NHS/SAM/ICE biosensor for aβ 1–42 detection, which provided a wide linear range of detection from 10^{-3}–10^{3} ng mL^{-1}, and a low limit of detection of aβ in HS (100 pg mL^{-1}) much lower than the limit of detection of CSF aβ 1–42 (~500 pg mL^{-1}), and other biosensors. Therefore, the developed biosensor is sensitive enough to be used for the diagnosis of early stage Alzheimer's disease.

1. Introduction

Alzheimer's disease (AD) is the most common form of dementia, defined as a group of symptoms associated with a decline in mental abilities, such as memory and reasoning. Pathological proteins of AD mainly include aβ peptide, and neurofibrillary tangles, formed from abnormally phosphorylated tau proteins within the cytoplasm of neurons (Gao et al., 2019; Kim et al., 2018; Chen et al., 2017; Rajasekhar et al., 2017; Yu et al., 2015). Their deposition leads to neuron damage by a series of pathways, resulting in memory and cognitive impairment (Awasthi et al., 2016; Wang and Mandelkow, 2015; Blennow and Zetterberg, 2009).

Diagnostic tools for the prediction of the staging of AD pathology such as positron emission tomography (PET) for amyloid deposits and magnetic resonance imaging (MRI) for mesial temporal lobe atrophy have been under development, and are being applied in clinical practice (Bullich et al., 2017; Morris et al., 2016; Madhavan et al., 2013; Dickerson et al., 2009). PET and MRI are expensive and have potential adverse side effects such as nausea, headache, vomiting, flushing, and itching. An alternate diagnostic approach is the detection of biomarkers in the cerebrospinal fluid (CSF). Studies have shown decreased levels and low concentrations of abnormal aβ 1–42 (a main of pathological proteins of AD), and increased levels of total tau (t-tau) and phosphorylated tau (p-tau) proteins (Blennow, 2017; Sperling et al., 2013; Gagni et al., 2013). However, the analysis of CSF biomarkers is an invasive procedure with a lumbar puncture and back pain. There is also high inter-laboratory variability of CSF biomarker analysis (Hampel et al., 2004; Irizarry, 2004). Therefore, cost-effective and feasible methods for the early diagnosis of aβ are required for AD management. For this, the analysis of blood (serum, plasma, or serum microRNA) biomarkers is of great interest (Azimzadeh et al., 2017; Jack et al., 2010; Perrin et al., 2009). Since blood biomarkers provide a rich source of proteomic species, this could help recognize AD earlier due to easy blood collection and analysis (Irizarry, 2004). Although blood-based biomarkers are an easy and less invasive method for the early diagnosis of AD, only a few studies have been done (Doecke et al., 2012; Apostolova et al., 2015). A better understanding of blood serum or plasma biomarkers is an important point in the early diagnosis of AD, and early detection of AD is the key to timely care measures to avoid illness and help prevent patients from decline.

Electrochemical biosensors have been proposed as an important strategy in biomarker sensing because of the rapid, sensitive, and selective detection capabilities of aβ at the pg mL^{-1} level (Qin et al., 2019; Xu et al., 2018; Rushworth et al., 2014; Ahn et al., 2011; Singh et al., 2019; Li et al., 2012; Chikae et al., 2008). Nano- or micro-interdigitated electrodes are highly recommended to enhance the sensing performance of biomarkers in a tiny sample volume, since the sensing area comparable to the size of analytes can be regulated by decreasing

---

[*] Corresponding author. Department of Electronics Engineering, Gachon University, 1342 Seongnamdaero, Sujeong-gu, Seongnam-si, Gyeonggi-do, 13120, South Korea.

E-mail address: sbcho@gachon.ac.kr (S. Cho).

https://doi.org/10.1016/j.bios.2019.111694
Received 19 July 2019; Received in revised form 5 September 2019; Accepted 6 September 2019

the gap between the interdigitated electrodes (Wang et al., 2017; Huang et al., 2014; Ino et al., 2011; Berggren et al., 2001). However, the sensing area is not homogenous in the typical rectangular-shaped interdigitated electrode because the electric fields highly concentrated at the edge of the rectangular electrode. If the edge effect of the electric fields distribution can be avoided by properly designing the electrode shape, it leads to improve the homogeneity of the sensing area on the electrodes and the reliability of the electrochemical sensor.

In this study, we fabricated the chain-shaped electrode to avoid the edge effect of the electric fields distribution and developed a highly sensitive electrochemical biosensor to detect aβ 1–42 peptide levels in human serum (HS). After immobilizing a specific anti-aβ antibody onto a self-assembled monolayer functionalized interdigitated chain-shaped electrode (ICE), the biosensor could detect aβ 1–42 in HS with a limit of detection of 100 pg mL^{-1}, much lower than the critical concentration value (~500 pg mL^{-1}) of CSF aβ 1–42. Compared with other assays (summarized in Table S1), our biosensor has several advantages, including a lower limit of detection and a wide linear range of detection of aβ 1–42 in HS, low cost, small size, and ease of operation. The selectivity of this system was also illustrated, with no significant interference from C-reactive protein, tumor necrosis factor-alpha, and insulin.

2. Materials and methods

2.1. Materials

6-Mercaptohexanoic acid (MHA, 90%), N-(3-dimethylaminopropyl)-N′ ethylcarbodiimide hydrochloride (EDC, crystalline), N-hydroxysuccinimide (NHS, 98.0%), bovine serum albumin (BSA), human serum (HS), potassium ferrocyanide ($K_4Fe(CN)_6$), potassium ferricyanide ($K_3Fe(CN)_6$) were purchased from Sigma-Aldrich (Korea). Amyloid-β 1–42 (aβ 1–42, human) peptide and anti-aβ antibody MOAB-2 were purchased from Abcam (Korea). Phosphate buffered saline (PBS, pH 7.4) was obtained from Tech and Innovation. De-ionized (DI) water (18.2 MΩ cm) was obtained from the Milli-Q system and used throughout the experiments.

2.2. Fabrication of interdigitated chain-shaped electrode (ICE)

The interdigitated chain-shaped electrode (ICE) was fabricated on a glass slide substrate (13.5 × 16.0 × 0.5 mm). An electrode thickness of 25 nm for titanium and 50 nm for gold were deposited by an electron beam evaporator, respectively. Afterwards, the paired electrode finger, which consists of 5 μm spacing and width for working, and reference electrodes were formed by the lift-off process. The design and a microscopic image of ICE containing gold fingers are shown in Fig. 1.

2.3. Development of the biosensor

The ICE was washed with pure ethanol, DI water, and dried in a N_2 stream to remove any impure materials from the electrode surface. MHA (50 mM) was attached to the cleaned ICE gold surface by incubation for 12 h, forming a self-assembled monolayer (SAM). The SAM-modified electrode was subsequently immersed in an EDC (75 mM)/NHS (5 mM) solution for antibody binding. Ten microliters of anti-aβ antibody (100 μg mL^{-1}) was drop-casted onto the modified electrode, and then kept in a humid chamber for 1 h to prevent drying of the surface during binding. The anti-aβ antibody was immobilized by a coupling reaction between the amino group of the anti-aβ antibodies and the EDC/NHS-activated MHA molecules on the modified electrodes. BSA (0.5% in 1X PBS, pH 7.4) was used to block nonspecific adsorption, forming the anti-aβ/EDC – NHS/SAM/ICE biosensor for detection of aβ 1–42 peptide (Fig. 1B).

2.4. Characterization of the SAM-modified electrode (SAM/ICE)

The surface morphology of the SAM/ICE was obtained by atomic force microscopy (AFM, PSIA XE-100, Park Systems, Korea), operated in non-contact mode, and scanned at a rate of 0.5 Hz. Energy-dispersive X-ray spectroscopy (EDS, S-4700, HITACHI, Japan) was used for the elemental analysis of samples. The surface morphology of the electrode was depicted by the 3D image and roughness between bare ICE and SAM-modified electrodes (Fig. 2).

2.5. Cyclic voltammetry

Cyclic voltammetry (CV) was used to characterize the electrochemical performances of the biosensor at various steps of the construction. Measurements were conducted using EC-Lab (Bio-Logic, sp-200, France) in a three-electrode configuration with the modified ICE as the working electrode, a platinum coil as the counter electrode and Ag/AgCl as the reference electrode in 5 mM ($K_4Fe(CN)_6$)/($K_3Fe(CN)_6$) (1:1 ratio) in PBS pH 7.4.

2.6. Electrochemical impedance spectroscopy (EIS)

Electrochemical impedance spectroscopy (EIS) was measured using EC-Lab (Bio-Logic, sp-200, France) in 5 mM ($K_4Fe(CN)_6$)/($K_3Fe(CN)_6$) (1:1 ratio) in PBS (pH 7.4) at each step of the biosensor construction. A bias voltage of 10 mV was applied between the working electrode (WE) and the reference electrode (RE) (Fig. 1) in the frequency range of 100

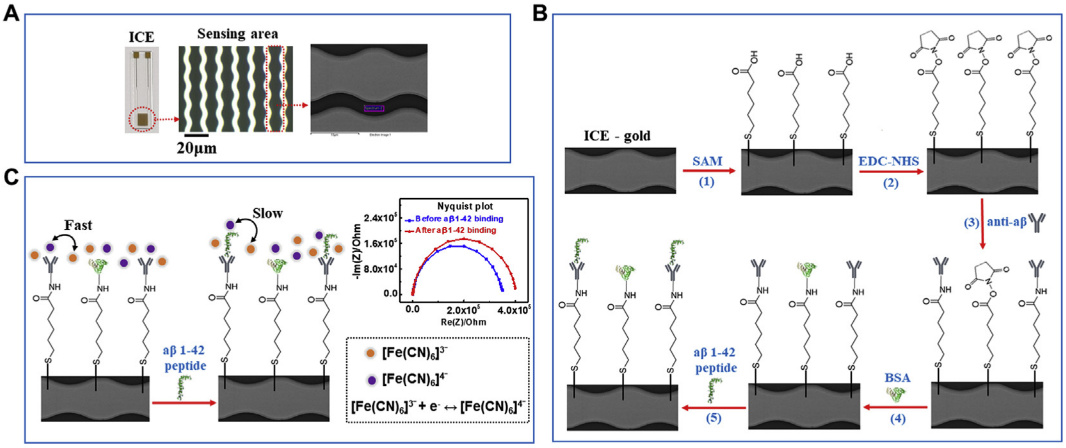

Fig. 1. (A) Microscopic image of the sensing fingers in ICE, (B) Schematic of the biosensor construction at each stage of the process, (C) The faradaic impedimetric surface engineering is based on the electron transfer resistance of the redox probe $[Fe(CN)_6]^{3-/4-}$ in solution.

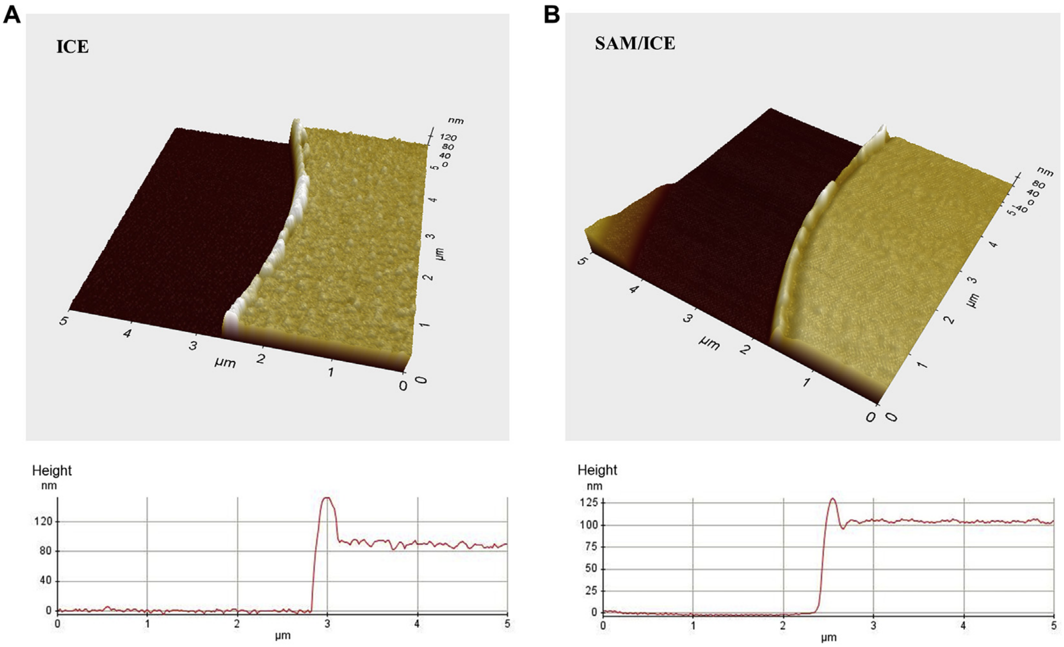

❖**ICE:** height (90.7 nm), roughness (2.4 nm)

❖**SAM/ICE:** height (104.1 nm), roughness (1.5 nm)

Fig. 2. AFM topographic profile of (A) bare ICE, and (B) the self-assembled monolayer-modified electrode (SAM/ICE).

mHz–1 MHz to record EIS performance. The anti-aβ/EDC–NHS/SAM/ICE biosensor was incubated in different concentrations of aβ (10^{-3}–10^{4} ng mL^{-1}) for 20 min at room temperature. After measurement with each concentration, the biosensor was washed with DI water and PBS before recording EIS in 5 mM ($K_4Fe(CN)_6$)/($K_3Fe(CN)_6$) in PBS pH 7.4. The obtained EIS data were fitted to the Randle's equivalent circuit model using ZView software (Southern Pines, USA).

3. Results and discussion

3.1. Electrochemical characterization of the anti-aβ/EDC–NHS/SAM/ICE biosensor

The biosensor fabrication is shown in (Fig. 1B). MHA was incubated on the gold surface of ICE (ICE-gold) to form a SAM as described in Section 2.3. AFM was used to characterize the morphology of the electrode surface along the deposition of the SAM. Fig. 2A and B shows the AFM 3D images from the glass substrate to gold electrode surface of bare ICE, and SAM/ICE. The formation of a smooth surface was observed after SAM deposition, which is demonstrated by the decreasing roughness of the electrode surfaces from 2.4 nm to 1.5 nm for bare ICE and SAM/ICE, respectively, confirming the changes in the electrode surface after SAM modification. The corresponding EDS results of the bare ICE and SAM/ICE are also exhibited in Fig. S1 (Supporting Information). The oxygen (O) atomic percentage increased to 36% and the sulfur (S) element increased to 1% after SAM deposition, indicating that the ICE-gold was successfully modified by the SAM via the strong affinity of sulfur for gold.

EIS was used to examine the deposition of materials to an electrode surface, investigate the surface interface and detect the changes to the biosensor surface through Nyquist complex-plane diagrams in the presence of 5 mM ($K_4Fe(CN)_6$)/($K_3Fe(CN)_6$) in PBS pH 7.4 over a frequency range 1 MHz–100 mHz (Fig. 3A). The semicircle diameter of the impedance spectra at each step of biosensor construction equals the interfacial charge-transfer resistance (R_{ct}). The fitting of the Nyquist plot data (Fig. 3A) to the Randle's equivalent circuit model (Fig. 3B) included the EIS parameters CPE (constant phase element for the electrode-solution interface), R_{ct} (charge-transfer resistance), and R_s (solution resistance). The R_{ct} value of the electrode changed after each layer of SAM, EDC–NHS, anti-aβ, BSA was deposited, respectively (Fig. 3C). The significant increase of R_{ct} after SAM immobilization is due to the –COO^{-} group and the carbon chain of the SAM which hinders the electron transfer of the negatively charged $[Fe(CN)_6]^{3^{-}/4^{-}}$ redox couple, corresponding to the significant decline of the current intensity in CV of the SAM compared to the bare ICE (Fig. 3D), resulting in the decrease of conductivity of the electrode after SAM deposition. Subsequently, the treatment of EDC–NHS on the SAM-modified electrode showed a decreased R_{ct} and an increase of current intensity in CV, demonstrating that the –COO^{-} groups of SAM were completely activated with EDC – NHS coupling. The R_{ct} increased again after the immobilization of anti-aβ and BSA due to the binding of a particular material on the biosensor surface which increased its surface resistance (Martic et al., 2013). The final steps of the biosensor construction, by addition of anti-aβ and BSA on the modified electrode surface, were also confirmed by CV (Fig. 3D).

3.2. Detection of aβ by the biosensor

The detection of aβ in a wide range of concentration from 10^{-3} ng mL^{-1} to 10^{4} ng mL^{-1} by the anti-aβ/EDC–NHS/SAM/ICE biosensor was described in Section 2.6. The EIS measurements of aβ incubation (10^{-3}–10^{4} ng mL^{-1}) are displayed as Nyquist plots in Fig. 4A with the imaginary component of impedance (-Im(Z)) plotted against the real component of impedance (Re(Z)). After using Randle's equivalent circuit model (Fig. 3B) to fit the obtained EIS data, the generated parameter R_{ct} could be used a parameter for the sensitive detection of aβ. The diameter and height of the semicircular Nyquist plots in Fig. 4A increased with the addition of increasing concentration of aβ (10^{-3}–10^{4} ng mL^{-1}), corresponding to increased R_{ct}. The R_{ct} enhanced gradually due to the binding of a specific amount of aβ from 10^{-3}–10^{4} ng mL^{-1} to the immobilized anti-aβ, leading to the hindering of electron transfer between the $[Fe(CN)_6]^{3^{-}/4^{-}}$ redox couple and the biosensor surface (Lien et al., 2015; Martic et al., 2013). The biosensor response to aβ was quantified as $(R_a - R_0)/R_0$ where R_0 represents the R_{ct} value of the biosensor with anti-aβ antibody deposition, and R_a represents the R_{ct} value of the biosensor with aβ (10^{-3}–10^{4} ng mL^{-1})

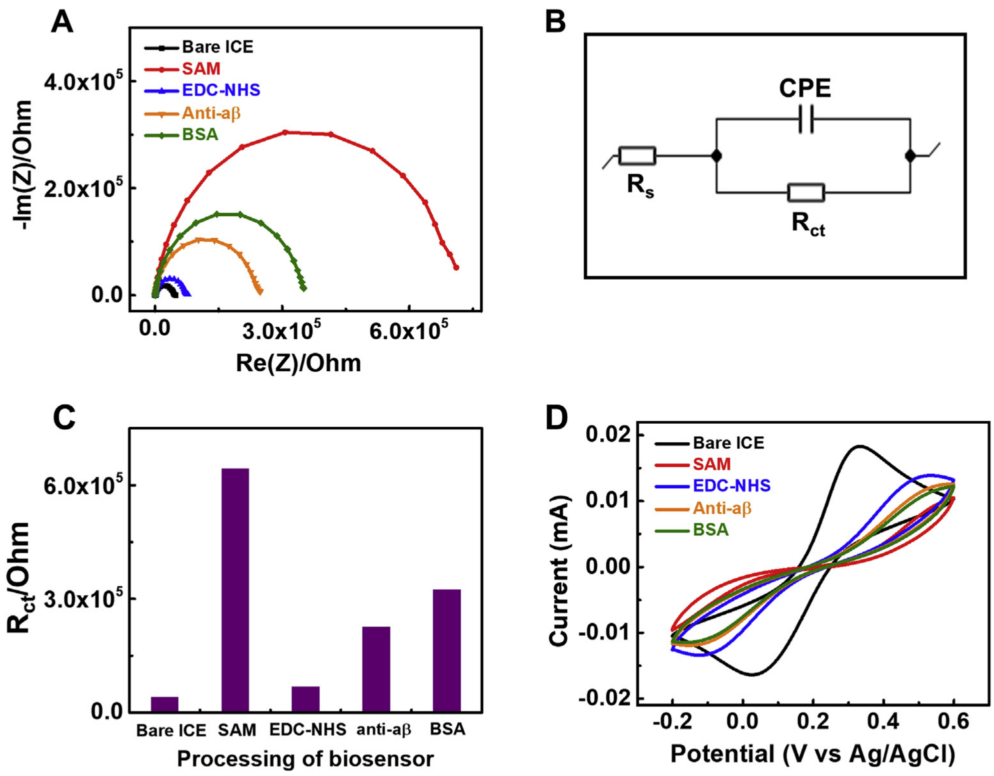

Fig. 3. Electrochemical characterization of the biosensor construction. (A) Nyquist plots at each stage of biosensor modification: bare ICE, SAM, EDC–NHS, anti-aβ, BSA in 10 mM $K_4Fe(CN)_6/K_3Fe(CN)_6$ (1:1 ratio) in PBS pH 7.4 in a frequency range of 1 MHz–100 mHz, (B) Randle's equivalent circuit model, (C, D) variance charge transfer resistance (R_{ct}) and CV at each stage of biosensor modification.

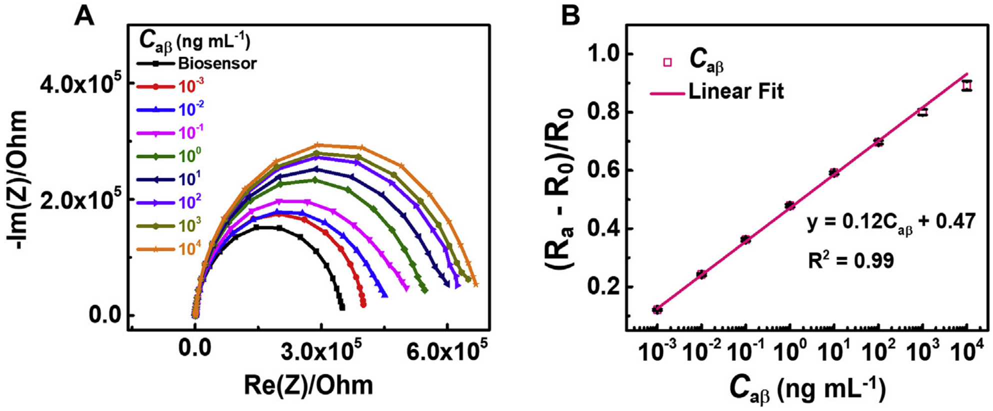

Fig. 4. Nyquist plots (A), and the calibration curve (B) of the biosensor after incubation with aβ (10^{-3}–10^4 ng mL^{-1}) in 5 mM $(K_4Fe(CN)_6)/(K_3Fe(CN)_6)$ (pH 7.4), R_0 and R_a are the value of R_{ct} measured without or with analyte, respectively; symbols and bars represent the average and standard deviation of the data (n = 3).

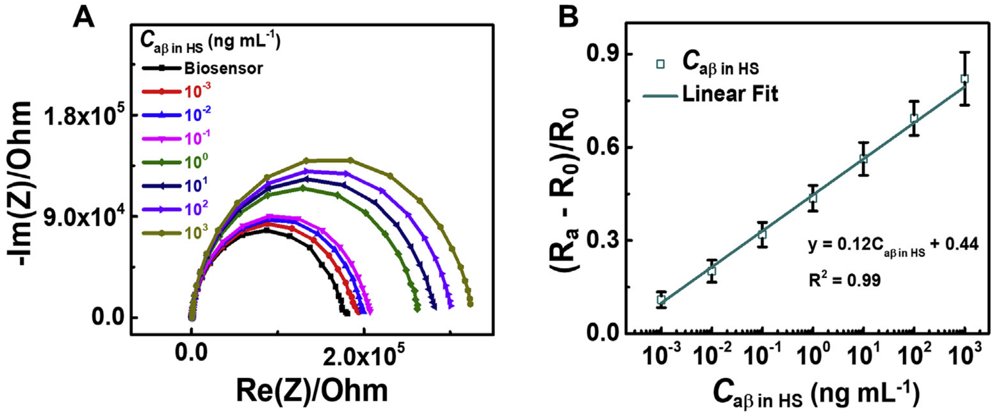

Fig. 5. Nyquist plots (A), and the calibration curve (B) of the biosensor after incubation with aβ (10^{-3}–10^3 ng mL^{-1}) in human serum (HS) with 5 mM $(K_4Fe(CN)_6)/(K_3Fe(CN)_6)$, R_0 and R_a are the value of R_{ct} measured without or with analyte, respectively; symbols and bars represent the average and standard deviation of the data (n = 3).

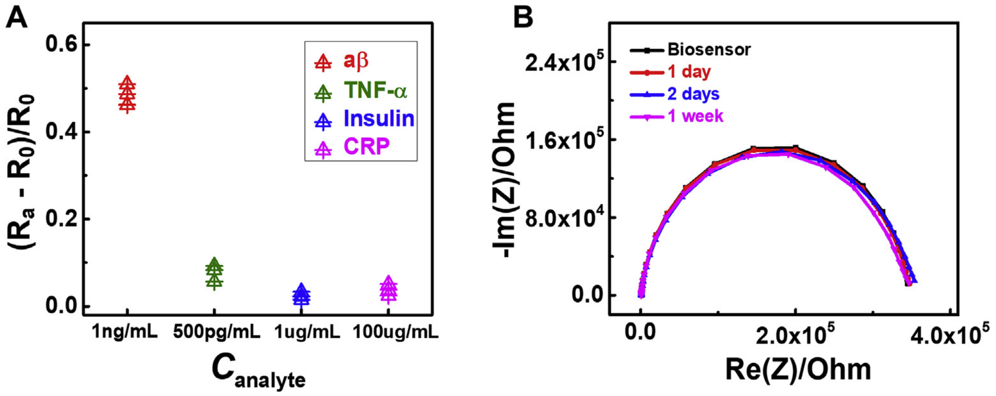

Fig. 6. Selectivity (A), and stability (B) of the biosensor, R_0 and R_a are the value of R_{ct} measured without or with analyte, respectively.

incubation (Fig. 4B). From the calibration curve in Fig. 4B, the limit of detection (LOD) calculated according to equation (3*S*/b) (Shrivastava and Gupta, 2011) where *S* is the standard deviation of the response and b is the slope of the calibration curve was 0.07 ng mL^{-1} (70 pg mL^{-1}), and the linear range of detection (LRD) was (10^{-3}–10^{3} ng mL^{-1}).

3.3. *Detection of aβ in HS by the biosensor*

We investigated the clinical capability of the anti-aβ/EDC–NHS/SAM/ICE biosensor for the detection of aβ in HS. Diluted HS (1:1000) was prepared by dilution of pure HS in 1 × PBS buffer pH 7.4 to avoid the matrix effects that make it difficult to get a robust calibration curve. Different aβ concentrations (10^{-3}–10^{3} ng mL^{-1}) were incubated with the biosensor in HS for 20 min, and the electrical impedance measurement was conducted in 5 mM ($K_4Fe(CN)_6$)/($K_3Fe(CN)_6$) over a frequency range of 1 MHz–100 mHz. The biosensor response to aβ in HS in Nyquist plots (Fig. 5A) exhibited the same tendency to that observed for aβ only (Fig. 4A), the R_{ct} increased with increasing aβ concentrations, demonstrating that the biosensor can detect aβ in HS. A calibration curve of the response of the biosensor to aβ is shown in Fig. 5B, and the LRD and LOD of the biosensor in HS were found to be (10^{-3}–10^{3} ng mL^{-1}) and 0.1 ng mL^{-1} (100 pg mL^{-1}), respectively. The anti-aβ/EDC–NHS/SAM/ICE biosensor presented a low LOD of aβ in both of HS and aβ only (100 and 70 pg mL^{-1}, respectively) compared to other aβ sensors that have been reported recently (see Table S1), affirming the application of the biosensor in clinical practice.

3.4. *Selectivity, interference, and stability tests*

To confirm the selectivity of the anti-aβ/EDC–NHS/SAM/ICE biosensor, the effect of three analytes, tumor necrosis factor-alpha (TNF-α, 500 pg mL^{-1}), insulin (1 μg mL^{-1}), and C-reactive protein (CRP, 100 μg mL^{-1}) in HS were studied by using the relationship between the interfacial resistance change and analyte concentration created from R_{ct} values from three independent experiments (Fig. 6A). The biosensor response to analytes in Fig. 6A was followed by $(R_a - R_0)/R_0$ where R_0 represents the R_{ct} value of the biosensor with anti-aβ antibody deposition, and R_a represents the R_{ct} value of the biosensor with TNF-α, insulin, or CRP incubation. The $(R_a - R_0)/R_0$ did not change much with incubation of TNF-α, insulin, or CRP compared to the response with incubation of aβ, demonstrating that there was no significant binding of anti-aβ antibody with CRP, TNF-α, or insulin. The change in R_a with incubation of aβ was due to specific antibody–antigen binding, indicating that the biosensor was selective for aβ detection. In addition, the interference study of TNF-α, insulin, or CRP along with aβ in HS was also displayed in Fig. S2. The $(R_a - R_0)/R_0$ maintains the same value after adding a certain amount of interferants, indicating that the presence of TNF-α, insulin, or CRP did not affect the detection of aβ in HS. EIS of the anti-aβ/EDC–NHS/SAM/ICE biosensor was maintained after 1 day, 2 days, and 1 week of storage at 4 °C (Fig. 6B), demonstrating the stability of the biosensor.

4. Conclusions

For sensing aβ 1–42 peptide, one of the AD biomarkers, we developed a low cost, small size, highly sensitive electrochemical biosensor based on immobilizing a specific anti-aβ antibody onto a self-assembled monolayer functionalized interdigitated chain-shaped electrode. Using the interdigitated chain-shaped electrode designed to improve the homogeneity of the sensing area, it was able to detect aβ 1–42 in the range of 10^{-3}–10^{3} ng mL^{-1} with a LOD of 100 pg mL^{-1} in HS, which was much lower than the LOD of CSF aβ 1–42 (~500 pg mL^{-1}) and other aβ 1–42 biosensors that have been proposed recently. This label-free and real-time impedimetric biosensor also demonstrated stability for one week of storage at 4 °C, and good selectivity of aβ 1–42 in HS including TNF-α, insulin, or CRP.

CRediT authorship contribution statement

Hien T. Ngoc Le: Conceptualization, Methodology, Validation, Formal analysis, Investigation, Writing - original draft. **Jinsoo Park:** Conceptualization, Methodology. **Somasekhar R. Chinnadayyala:** Conceptualization, Methodology. **Sungbo Cho:** Conceptualization, Methodology, Resources, Writing - review & editing, Supervision, Project administration, Funding acquisition.

Declaration of competing interest

The authors declare that they have no known competing financial interests or personal relationships that could have appeared to influence the work reported in this paper.

Acknowledgments

The work was supported by the National Research Foundation of Korea, Republic of Korea. (Grant No. NRF 2017R1D1A1A09000712, 2018M3A9F1023690, and 2018M3A9F1023691).

Appendix A. Supplementary data

Supplementary data to this article can be found online at https://doi.org/10.1016/j.bios.2019.111694.

References

Ahn, J., Lee, T.H., Li, T., Heo, K., Hong, S., Ko, J., Kim, Y., Shin, Y.B., Kim, M.G., 2011. Biosens. Bioelectron. 26, 4690–4696.
Apostolova, L.G., Hwang, K.S., Avila, D., Elashoff, D., Kohannim, O., Teng, E., Sokolow,

S., Jack, C.R., Jagust, W.J., Shaw, L., et al., 2015. Neurology 84, 729–737.
Awasthi, M., Singh, S., Pandey, V.P., Dwivedi, U.N., 2016. J. Neurol. Sci. 361, 256–271.
Azimzadeh, M., Nasirizadeh, N., Rahaie, M., Naderi-Manesh, H., 2017. RSC Adv. 7, 55709–55719.
Berggren, C., Bjarnason, B., Johansson, G., 2001. Electroanalysis 13, 173–180.
Blennow, K., 2017. Neurol Ther 6, 15–24.
Blennow, K., Zetterberg, H., 2009. J. Alzheim. Dis 413, 417.
Bullich, S., Seibyl, J., Catafau, A.M., Jovalekic, A., Koglin, N., Barthel, H., Sabri, O., DeSanti, S., 2017. Neuroimage Clin 15, 325–332.
Chen, G.F., Xu, T.H., Yan, Y., Zhou, Y.R., Jiang, Y., Melcher, K., Xu, H.E., 2017. Acta Pharmacologica Sinica. pp. 1205–1235.
Chikae, M., Fukuda, T., Kerman, K., Idegami, Miura, K.Y., Tamiya, E., 2008. Bioelectrochemistry 74, 118–123.
Dickerson, B.C., Bakkour, A., Salat, D.H., Feczko, E., Pacheco, J., Greve, D.N., Grodstein, F., Wright, C.I., Blacker, D., Rosas, H.D., Sperling, R.A., Atri, A., Growdon, J.H., Hyman, B.T., Morris, J.C., Fischl, B., Buckner, R.L., 2009. Cerebr. Cortex 19, 497–510.
Doecke, J.D., Laws, S.M., Faux, N.G., et al., 2012. Arch. Neurol. 69, 1318–1325.
Gagni, P., Sola, L., Cretich, M., Chiari, M., 2013. Biosens. Bioelectron. 47, 490–495.
Gao, F., Gao, K., He, C., Liu, M., Wan, H., Wang, P., 2019. Biosens. Bioelectron. 133, 183–191.
Hampel, H., Teipel, S.J., Fuchsberger, T., Andreasen, N., Wiltfang, J., Otto, M., Shen, Y., Dodel, R., Du, Y., Farlow, M., et al., 2004. Mol. Psychiatry 9, 705–710.
Huang, S.Y., Chou, C.M., Chen, T.H., Chiou, P.C., Hsiao, V.K.S., Ching, C.T.S., Sun, T.P., 2014. J. Electrochem. Soc. 161, B102–B105.
Ino, K., Saito, W., Koide, M., Umemura, T., Shiku, H., Matsue, T., 2011. Lab Chip 11, 385–388.
Irizarry, M.C., 2004. NeuroRx 1, 226–234.
Jack Jr., C.R., Knopman, D.S., Jagust, W.J., Shaw, L.M., Aisen, P.S., Weiner, M.W., Petersen, R.C., Trojanowski, J.Q., 2010. Lancet Neurol. 9, 119–128.
Kim, H.B., Lee, J.U., Song, S.J., Kim, S.H., Sim, S.J., 2018. Biosens. Bioelectron. 101, 96–102.
Li, H., Cao, Y., Wu, X., Ye, Z., Li, G., 2012. Talanta 93, 358–363.
Lien, T.T.N., Takamura, Y., Tamiya, E., Vestergaard, M.C., 2015. Anal. Chim. Acta 892, 69–76.
Madhavan, A., Whitwell, J.L., Weigand, S.D., Duffy, J.R., Strand, E.A., Machulda, M.M., Tosakulwong, N., Senjem, M.L., Gunter, J.L., Lowe, V.J., Petersen, R.C., Jack Jr., C.R., Josephs, K.A., 2013. PLoS One 8, 62471.
Martic, S., Rains, M.K., Kraatz, H.B., 2013. Anal. Biochem 442, 130–137.
Morris, E., Chalkidou, A., Hammers, A., Peacock, J., Summers, J., Keevil, S., 2016. Eur. J. Nucl. Med. Mol. Imaging 43, 374–385.
Perrin, R.J., Fagan, A.M., Holtzman, D.M., 2009. Nature 461, 916–922.
Qin, H.X., Gao, X., Yang, X.Y., Cao, W., Liu, S.F., 2019. Biosens. Bioelectron. 141, 111438.
Rajasekhar, K., Narayanaswamy, N., ArulMurugan, N., Viccaro, K., Lee, H.G., Shah, K., Govindaraju, T., 2017. Biosens. Bioelectron. 98, 54–61.
Rushworth, J.V., Ahmed, A., Griffiths, H.H., Pollock, N.M., Hooper, N.M., Millner, P.A., 2014. Biosens. Bioelectron. 56, 83–90.
Shrivastava, A., Gupta, V.B., 2011. Chronicles Young Sci. 2.
Singh, S., Gill, A.A.S., Nlooto, M., Karpoormath, R., 2019. Biosens. Bioelectron. 137, 213–221.
Sperling, R.A., Karlawish, J., Johnson, K.A., 2013. Nat. Rev. Neurol. 9, 54–58.
Wang, L., Veselinovic, M., Yang, L., Geiss, B.J., Dandy, D.S., Chen, T., 2017. Biosens. Bioelectron. 87, 646–653.
Wang, Y., Mandelkow, E., 2015. Nat. Rev. Neurosci. 17, 22–35.
Xu, R., Wei, D., Du, B., Cao, W., Fan, D.W., Zhang, Y., Wei, Q., Ju, H.X., 2018. Biosens. Bioelectron. 122, 37–42.
Yu, Y., Sun, X., Tang, D., Li, C., Zhang, L., Nie, D., Yin, X., Shi, G., 2015. Biosens. Bioelectron. 68, 115–121.